Biochemical Characterization of Mono(ADP-ribosyl)ated Poly(ADP-ribose) Polymerase†

Hilda Mendoza-Alvarez and Rafael Alvarez-Gonzalez*

Department of Molecular Biology and Immunology, University of North Texas Health Science Center at Fort Worth, Fort Worth, Texas 76107-2699

Received September 4, 1998; Revised Manuscript Received December 23, 1998

ABSTRACT: Here, we report the biochemical characterization of mono(ADP-ribosyl)ated poly(ADP-ribose) polymerase (PARP) (EC 2.4.2.30). PARP was effectively mono(ADP-ribosyl)ated both in solution and via an activity gel assay following SDS−PAGE with 20 μM or lower concentrations of [^{32}P]-3′-dNAD$^+$ as the ADP-ribosylation substrate. We observed the exclusive formation of [^{32}P]-3′-dAMP and no polymeric ADP-ribose molecules following chemical release of enzyme-bound ADP-ribose units and high-resolution polyacrylamide gel electrophoresis. The reaction in solution (i) was time-dependent, (ii) was activated by nicked dsDNA, and (iii) increased with the square of the enzyme concentration. Stoichiometric analysis of the reaction indicated that up to four amino acid residues per mole of enzyme were covalently modified with single units of 3′-dADP-ribose. Peptide mapping of mono(3′-dADP-ribosyl)ated-PARP following limited proteolysis with either papain or α-chymotrypsin indicated that the amino acid acceptor sites for chain initiation with 3′-dNAD$^+$ as a substrate are localized within an internal 22 kDa automodification domain. Neither the amino-terminal DNA-binding domain nor the carboxy-terminal catalytic fragment became ADP-ribosylated with [^{32}P]-3′-dNAD$^+$ as a substrate. Finally, the apparent rate constant of mono-(ADP-ribosyl)ation in solution indicates that the initiation reaction catalyzed by PARP proceeds 232-fold more slowly than ADP-ribose polymerization.

The poly(ADP-ribosyl)ation of DNA-binding proteins in chromatin is a postranslational covalent modification reaction catalyzed by poly(ADP-ribose) polymerase (PARP) (EC 2.4.2.30) in higher eucaryotes *(1, 2)*. The purified enzyme is a single polypeptide of 1014 amino acid residues (113 kDa) which exhibits an absolute requirement for dsDNA *(1, 2)* containing nicks or breaks *(3, 4)*. Although several chromatin proteins are efficient poly(ADP-ribose) acceptors, including histone and non-histone proteins *(1, 2)*, by far the main protein target for poly(ADP-ribosyl)ation in vitro *(5, 6)* and in vivo *(7, 8)* is PARP itself. Some reports in the literature suggest that anywhere from 15 *(9)* to 28 *(10)* amino acid residues of PARP may function as acceptor sites for covalent automodification. The automodification reaction of PARP appears to be a prerequisite for the efficient repair of DNA damage following exposure of mammalian cells to alkylating agents *(11)*. These and other experimental observations *(12)* suggest that the auto-poly(ADP-ribosyl)ation reaction catalyzed by PARP is of fundamental importance in chromatin structure and function as well as in cell survival *(13)*.

Although the regulatory mechanism of the automodification of PARP has not been completely elucidated, recent results indicate that two types of macromolecular interactions are involved in this process, namely, (i) PARP−DNA and (ii) PARP−PARP interactions. Noncovalent interactions of PARP with nicked dsDNA have recently been observed by electron microscopy *(14)* where a stable V-shaped DNA is formed when two molecules of PARP bind to each free end of a single DNA strand break. In addition, chemical cross-linking experiments have also shown that PARP has a strong tendency for self-association *(15)*. In consistency with this notion, a physicochemical analysis of the auto-poly(ADP-ribosyl)ation reaction of PARP also revealed that this enzyme functions as a catalytic dimer during ADP-ribose polymerization *(16)*. Indeed, the highest enzymatic activity of PARP was displayed when the ratio of PARP/DNA was equal to 2 *(17)*.

To better understand the regulation of PARP, we have manipulated the conditions of our in vitro purified enzyme system to slow the automodification reaction to dissect poly-(ADP-ribose) synthesis into individual steps of initiation, elongation, and branching *(16, 18)*. Initially, our goal was partially achieved by manipulating the concentration of βNAD$^+$ in the assay, e.g., nanomolar vs micromolar concentrations (*16*). While mono(ADP-ribosyl)ated PARP was the main product at 200 nM βNAD$^+$, some oligo(ADP-ribosyl)ation was always present *(16)*. Addition of competitive inhibitors of ADP-ribose polymerization, e.g., benzamide, also slowed this reaction into individual steps of initiation, elongation, and branching (*18*). However, less than 1% of the enzyme activity was observed at high benzamide/βNAD$^+$ ratios *(18)*.

A full understanding of the regulatory mechanism(s) of PARP requires the complete characterization of each reaction catalyzed by this enzyme. Here, we have used 3′-deoxy-

†This project was fully supported by Grant GM45451 from the National Institutes of Health.

* Address correspondence to this author. Tel: (817) 735-2117. Fax: (817) 735-2133. E-mail: ralvarez@hsc.unt.edu.

10.1021/bi982148p CCC: $18.00
Published on Web 03/09/1999

NAD^+ (3′-dNAD$^+$) as a substrate to characterize the auto-mono(ADP-ribosyl)ation reaction catalyzed by PARP (chain initiation). Incubations of either immobilized PARP (activity gels) or enzyme solutions with 20 μM 3′-dNAD$^+$ (or lower substrate concentrations) resulted in the exclusive mono(3′-dADP-ribosyl)ation of the enzyme.

EXPERIMENTAL PROCEDURES

Chemicals and Materials. Hydroxyapatite (HPT Bio-Gel), electrophoresis molecular mass markers, and electrophoresis reagents were purchased from Bio-Rad (Hercules, CA); Sephadex G-25 and Ultrogel 45 were obtained from Pharmacia LKB Biotechnology Inc. (Piscataway, NJ); Matrex-Gel Red A was obtained from Amicon (Beverly, MA); cellulose, Partisil 10-SAX columns, and packing material were bought from Whatman, Inc. (Fairfield, NJ); inorganic pyrophosphatase, alkaline phosphatase type II-S, dithiothreitol, lithium dodecyl sulfate (LDS), and active calf thymus DNA were obtained from Sigma (St. Louis, MO); [α-^{32}P]-3′-dATP (specific activity 5000 Ci/mmol) was purchased from NEN (Boston, MA); all other chemicals used were of the highest purity commercially available.

Enzyme Purification. PARP was purified from calf thymus as previously described *(19)*.

Synthesis and Purification of 3′-dNAD$^+$. Radiolabeled 3′-dNAD$^+$ was synthesized by a previously published procedure *(20)*. Briefly, 1 mCi of [α-^{32}P]-3′-dATP was incubated with 3 units of inorganic pyrophosphatase and 0.2 unit of NAD pyrophosphorylase in the presence of 3 mM NMN^+, 10 mM $MgCl_2$, and 100 mM glycylglycine buffer, pH 7.4, for 2 h at 37 °C. The reaction product was purified by (i) boronate chromatography and (ii) high-performance liquid chromatography (HPLC) on a Partisil 10-SAX column. The concentration of pure ^{32}P-radiolabeled 3′-dNAD$^+$ was determined either by specific radioactivity measurements or by absorbance at 254 nm.

Activity Gel Analysis of Poly(ADP-ribose) Polymerase. Functional PARP, endogenous to rat liver chromatin *(21)*, was recovered by the removal of SDS from a 7% polyacrylamide gel containing 20 μg/mL DNA. Following removal of the detergent, the gel was renatured by shaking gently for 16−18 h at 4 °C in 50 mM Tris-HCl, pH 8.0, 3 mM 2-mercaptoethanol, and 6 M guanidine hydrochloride *(22)*. Afterward, the in situ assay for PARP was carried out by incubating the intact gel for 9−12 h at 37 °C with 10 mL of 100 mM Tris-HCl, pH 8.0, 10 mM $MgCl_2$, 1 mM dithiothreitol, and 10 μCi/mL [^{32}P]-3′-dNAD$^+$. After the reaction was completed, the gel was washed with ice-cold 5% TCA until background radioactivity in the wash fell below 1000 cpm/mL. Gels were exposed to Kodak XAR-2 film for autoradiographic processing.

Auto-mono(3′-dADP-ribosyl)ation of PARP in Solution. The reaction mixture for the auto-mono(3′-dADP-ribosyl)-ation of PARP contained 200 ng of PARP (~2 pmol of enzyme), 20 μM [^{32}P]-3′-dNAD$^+$, 20 μg/mL activated DNA, 100 mM Tris-HCl, pH 7.8, 10 mM $MgCl_2$, and 1 mM dithiothreitol in a total volume of 100 μL. The reaction was incubated at 37 °C. Short times of incubation resulted in very low levels of substrate incorporation which hindered the quantification of the enzyme rates by liquid scintillation counting. PARP activity was determined by measuring the total amount of ^{32}P incorporated into 20% (w/v) trichloroacetic acid (TCA) insoluble material. The rates of auto-mono-(3′-dADP-ribosyl)ation (picomoles incorporated per minute) were calculated and plotted versus (i) [DNA], (ii) [PARP], or (iii) [3′-dNAD$^+$].

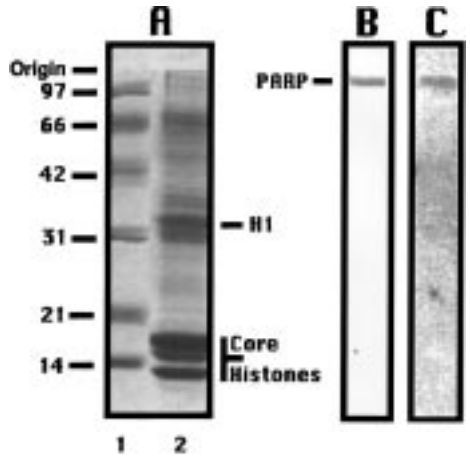

FIGURE 1: Auto-mono(ADP-ribosyl)ation of immobilized rat liver chromatin PARP via an activity gel assay (panel A, lane 2) with either [^{32}P]NAD$^+$ (panel B) or [^{32}P]-3′-dNAD$^+$ (panel C) as the substrate. The electrophoretic migration of the molecular mass markers is shown on panel A, lane 1.

Proteolytic Digestion of PARP with Papain and/or α-Chymotrypsin. A purified preparation of PARP from calf thymus (500 μg/mL) *(19)* was digested at 0 °C with papain (20:1). After a few minutes of enzymatic digestion, the reaction was terminated with 20% ice-cold TCA. Proteolysis with α-chymotrypsin was carried out for 20 min at 25 °C and stopped with 1 mM phenylmethanesulfonyl fluoride. Sequential proteolytic treatment was performed with α-chymotrypsin first and papain last.

LDS−Polyacrylamide Gel Electrophoresis. ADP-ribosylated proteins were dissolved in 2× electrophoresis buffer containing 1% LDS, the samples were boiled for 5 min and loaded onto a 7% polyacrylamide gel containing 0.1% LDS instead of SDS at pH 6.8 to stabilize the monoester bonds of the poly(ADP-ribose)−protein conjugates, and electrophoresis was carried out as reported elsewhere *(23)*.

Size Distribution of Enzyme-Bound ADP-ribose Chains by High-Resolution Polyacrylamide Gel Electrophoresis. Acid-precipitable material was processed for analysis of the ADP-ribose chains by electrophoresis on 20% polyacrylamide gels *(24)*. Briefly, the [^{32}P]ADP-ribose chains were chemically detached from PARP with 0.1 N NaOH and 20 mM EDTA for 2 h at 60 °C, neutralized with 0.1 N HCl, diluted in 60 mM Tris−borate−EDTA (TBE) buffer, pH 8.3, and subjected to electrophoresis on a 20 × 20 cm long gel. Gels were exposed to Kodak (XAR-2) X-ray film for autoradiography.

RESULTS

We previously reported that PARP efficiently catalyzes an automodification reaction with 3′-dNAD$^+$ as an ADP-ribosylation substrate *(23)*. In fact, the enzyme synthesized PARP-bound oligomers of 3′-dADP-ribose in solution with 40−120 μM substrate concentrations *(23)*. Now, we have carried out the automodification of immobilized PARP with this NAD^+ analogue via an activity gel assay *(22)*. Figure 1

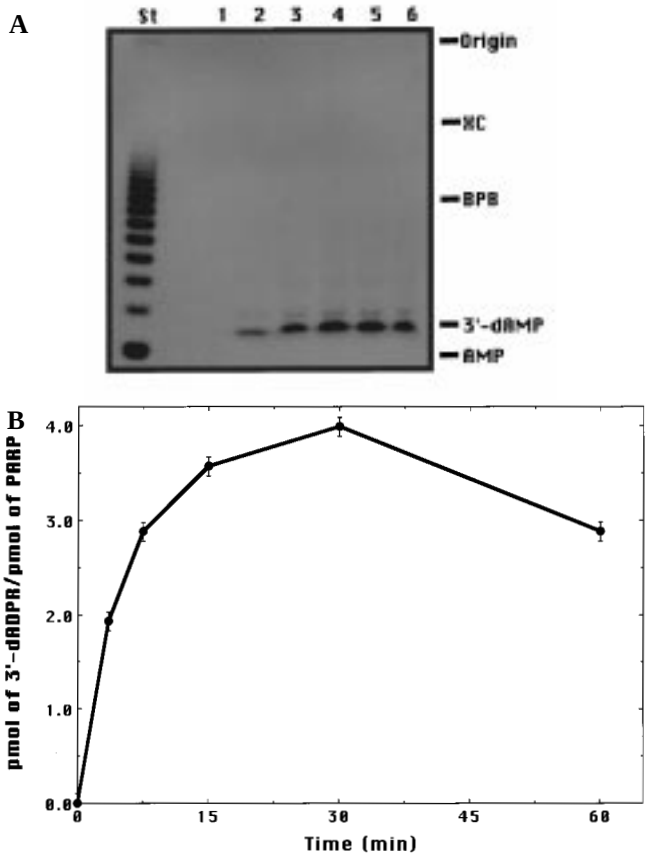

FIGURE 2: Kinetics and stoichiometry of the auto-mono(ADP-ribosyl)ation of PARP in solution with [^{32}P]-3′-dNAD$^+$ as a substrate. Panel A shows the chain length of the 3′-dADP-ribose units released from PARP following alkaline treatment in the presence of EDTA. The electrophoretic migration of ADP-ribose chains of increasing lengths is shown to the left of the autoradiograph (St), and the relative migration of xylene cyanol or XC (which runs with a 20-mer) and bromophenol blue or BPB which comigrates with an 8-mer as well as that of 3′-dAMP and AMP is shown to the right. Lanes 1 through 6 show the products generated after 3, 7.5, 15, 30, and 60 min of automodification. Panel B shows the kinetics and stoichiometry of the auto-mono(ADP-ribosyl)ation reaction of PARP. Error bars show the average of duplicate measurements.

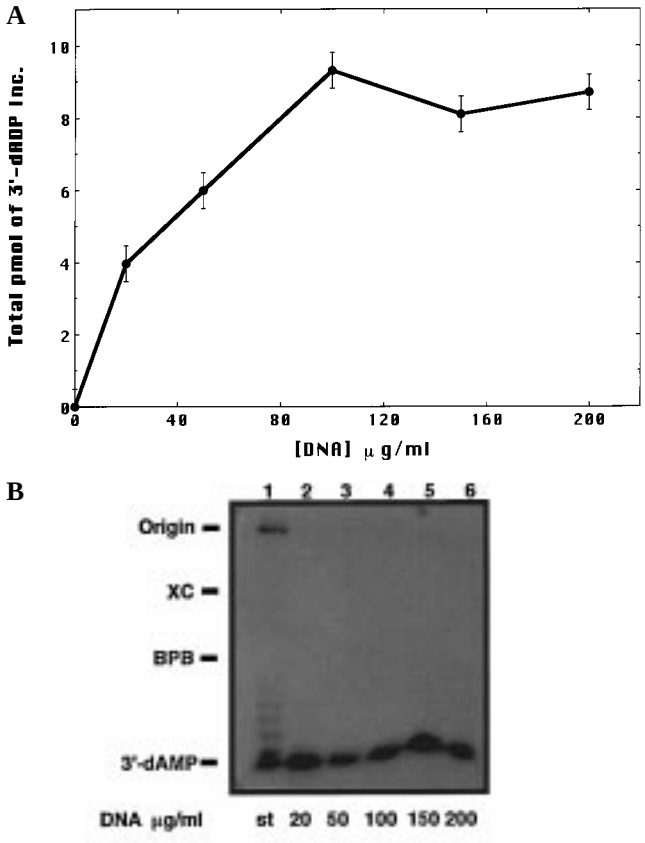

FIGURE 3: Dose-dependent activation of the auto-mono(ADP-ribosyl)ation of PARP by nicked dsDNA. Panel A shows the total picomoles of 3′-dADP-ribose incorporated as a function of the nicked dsDNA concentration (3 min incubations). Error bars show the average of duplicate measurements. Panel B shows the chain length of the 3′-dADP-ribose units released from PARP following alkaline treatment in the presence of EDTA. The electrophoretic migration of ADP-ribose chains of increasing lengths is shown to the left of the autoradiograph (lane 1), and the relative migration of xylene cyanol or XC (which runs with a 20-mer) and bromophenol blue or BPB which comigrates with an 8-mer as well as that of 3′-dAMP is also shown to the left. The concentration of nicked dsDNA in the assay is shown below the autoradiograph.

shows that a radiolabeled protein band electrophoresed at the position of PARP following incubation of rat liver chromatin *(21)* (panel A, lane 2) with either [^{32}P]-3′-dNAD$^+$ (panel C) or [^{32}P]NAD$^+$ (panel B) after electrophoresis in an 7% SDS-polyacrylamide gel containing 20 μg/mL active DNA as indicated in Experimental Procedures *(23)*. Unexpectedly, when the concentration of this NAD$^+$ analogue is kept at 20 μM or lower concentrations, the only enzymatic product observed was mono(3′-dADP-ribosyl)ated PARP. Figure 2A shows the autoradiographic analysis of the 3′-dADP-ribose chains synthesized with 20 μM 3′-dNAD$^+$ as a function of time following chemical release from PARP. In these assays, a single radiolabeled band of 3′-dAMP was observed even after 30 min of automodification. It should be pointed out that, at 60 min of incubation or longer, small amounts of 3′-dADP-ribose oligomerization are detected upon long autoradiographic exposures. Also shown in Figure 2A, lane St, is the ladder of ADP-ribose chains synthesized by PARP with [^{32}P]βNAD$^+$ as a substrate (control). Our results are consistent with the conclusion that 3′-dNAD$^+$ is an efficient chain terminator of ADP-ribose polymerization.

To better document the kinetics of this reaction, we next determined the stoichiometry of the reaction in 100 μL incubations with 2 pmol of PARP (~220 ng) and 20 μM 3′-dNAD$^+$. Figure 2B shows that the total amount of substrate incorporated into enzyme-bound form increases with time. The level of auto-mono(ADP-ribosyl)ation displayed by PARP plateaus at 4 pmol of monomeric 3′-dADP-ribose/pmol of PARP. Therefore, a maximum of 8 mol of monomeric 3′-dADP-ribose is incorporated into enzyme-bound form per catalytic complex (dimer).

In 1980, it was demonstrated that the ADP-ribose polymerizing activity associated with PARP is greatly enhanced by dsDNA containing nicks or breaks *(3)*. Later, we and others demonstrated that this was the result of enzymatic dimerization on the DNA strand break *(14−17)*. Therefore, we next examined the effect of nicked dsDNA on the auto-mono(ADP-ribosyl)ation reaction of PARP alone. Figure 3A shows that the levels of mono(ADP-ribosyl)ation of PARP increased as a function of the concentration of nicked dsDNA with substrate saturation kinetics. Unexpectedly, the autoradiographic profile of the protein-free 3′-dADP-ribose residues revealed that 3′-dAMP was the only radiolabeled product chemically released from the enzyme regardless of

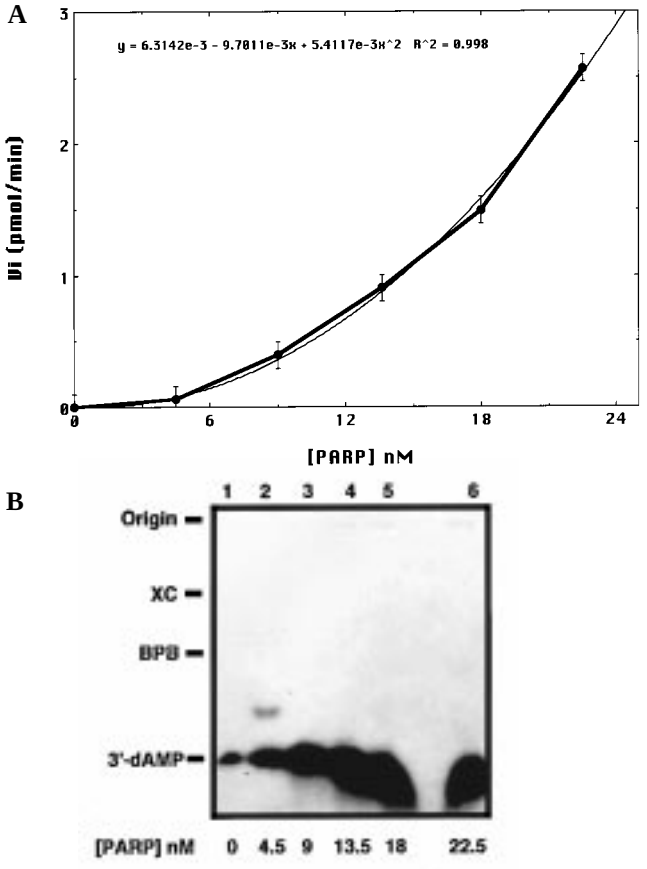

FIGURE 4: The auto-mono(ADP-ribosyl)ation reaction of PARP is enzyme concentration-dependent. Panel A shows the initial rates (3 min incubations) as a function of the concentration of PARP. Error bars show the average of triplicate measurements of three separate experiments. Panel B shows the chain length of the 3′-dADP-ribose units released from PARP following alkaline treatment in the presence of EDTA. The electrophoretic migration of xylene cyanol or XC (which runs with a 20-mer) and bromophenol blue or BPB which comigrates with an 8-mer as well as that of 3′-dAMP is also shown to the left. The nanomolar concentration of PARP in the assay is shown below the autoradiograph.

the concentration of nicked dsDNA utilized (Figure 3B). Therefore, nicked dsDNA enhances the mono(ADP-ribosyl)-transferase activity associated with PARP independently of its effect on chain elongation *(3)* when NAD^+ is used as a substrate. Afterward, we determined the dependence of the auto-mono(3′-dADP-ribosyl)ation as a function of enzyme concentration at a constant ratio of dsDNA (20 μg/mL) to 3′-$dNAD^+$ (20 μM). In these experiments, we observed that the rates of chain initiation increased with the square of the enzyme concentration (Figure 4A). Thus, we conclude that a dimer of PARP is involved in ADP-ribose chain initiation and that this reaction takes place intermolecularly. Once again, [^{32}P]-3′-dAMP was the only product observed following alkaline release from PARP regardless of the enzyme concentration used in the assay (Figure 4B). A careful kinetic evaluation of a Hanes−Wilkinson plot (not shown) reflected that the initiation reaction of PARP with 3′-$dNAD^+$ as a substrate proceeded with an apparent *Km* of PARP for 3′-$dNAD^+$ of 12.6 ± 3.0 μM, a k_{cat} of 0.33/min, and a k_{cat}/k_m = 436.5. By contrast, the ADP-ribose polymerization reaction with [^{32}P]NAD^+ as a substrate (*16*) displayed (i) an apparent K_{NAD} = 59 μM, (ii) a k_{cat} = 77.4/min, and (iii) k_{cat}/K_{NAD} = 2.18 × 10^4 *(16)*. These results indicated that the mono(ADP-ribosyl)transferase activity associated with PARP is 230 times slower than ADP-ribose polymerization and that the enzyme efficiency is 50-fold less than chain elongation. Interestingly, the incubation of PARP with 40 μM or higher concentrations of 3′-$dNAD^+$ revealed limited chain elongation to tetramers and pentamers of 3′-dADP-ribose (data not shown).

To further characterize the auto-mono(ADP-ribosyl)ation of PARP with low micromolar concentrations of 3′-$dNAD^+$, we proceeded to identify the peptide domain(s) of PARP that function(s) as a target for the ADP-ribose chain initiation reaction. To accomplish this objective, we subjected PARP to limited proteolysis with either α-chymotrypsin, papain, or both *(25−27)*. Treatment with α-chymotrypsin primarily generated a 54 kDa amino-terminal fragment (which further proteolyzed down into 40 kDa and 14 kDa peptide fragments, half-closed arrows) and a more stable 66 kDa carboxy-terminal domain (Figure 5A, lane 2, closed arrows). Of these fragments, only the 66 kDa carboxy terminus was radiolabeled (Figure 5B, lane 2), as judged by autoradiography of the LDS gel (vide supra). By contrast, treatment of mono-(ADP-ribosyl)ated PARP with papain generated a 46 kDa amino-terminal DNA-binding domain *(25)* and a 74 kDa carboxy-terminal catalytic domain (Figure 5A, lane 3, open arrows). Autoradiographic analysis of this reaction mixture (Figure 5B, lane 3) also revealed that only the 74 kDa carboxy-terminal fragment containing the automodification and catalytic domains was radiolabeled. Finally, Figure 5A, lane 4, shows that the sequential treatment of mono(ADP-ribosyl)ated PARP with papain and α-chymotrypsin generated a 22 kDa peptide that electrophoreses at the position of the automodification peptide fragment of PARP *(27)*. Surprisingly, this proteolytic product of PARP corresponds to the main radiolabeled peptide fragment observed by autoradiography following electrophoresis on an LDS gel (Figure 5B, lane 4). Lanes 1 of panels A and B of Figure 5 both show the electrophoretic migration of mono(ADP-ribosyl)-ated PARP as the nonproteolyzed control.

DISCUSSION

Poly(ADP-ribose) polymerase (PARP) is a highly versatile eucaryotic enzyme associated with chromatin that is capable of catalyzing the covalent attachment of an ADP-ribose residue from βNAD^+ to Glu residues on histone, non-histone proteins, and itself *(1, 2)*. This reaction therefore generates monoesterified products e.g., mono(ADP-ribosyl)ated protein(s), which can be further elongated to polymeric molecules of over 200 residues in size *(24)*. Therefore, this enzyme also catalyzes the formation of the 2′−1″ ribose−ribose bond (chain elongation) *(16, 23, 24, 28)* and the 2″−1‴ ribose−ribose bond (branching step) *(28)* of poly(ADP-ribose) synthesis with high efficiency. The synthesis of long and highly branched ADP-ribose polymers *(24)* requires protein−protein interactions (via homo- or heterodimer formation) *(14−17)* on nicked or broken dsDNA *(3, 4)*. While the synthesis of short ADP-ribose oligomers (no more than four residues) with 40 μM or higher levels of 3′-$dNAD^+$ has previously been reported *(23)*, very little is known about the role of protein−protein, protein−DNA, and protein−substrate interactions in the biochemical regulation of this enzyme. Here, we have observed that the incubation of soluble and immobilized PARP with 20 μM 3′-$dNAD^+$

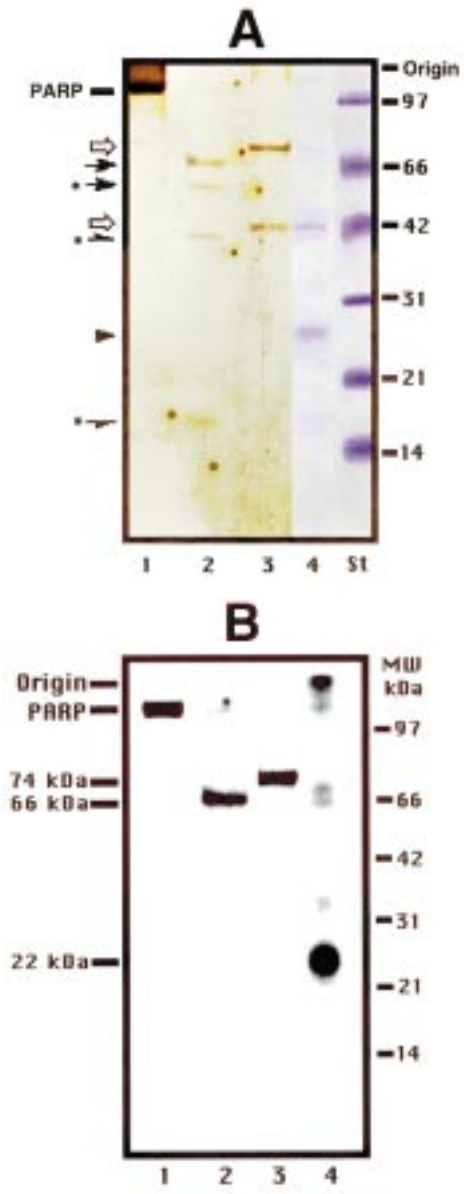

FIGURE 5: The initiation reaction catalyzed by PARP with [^{32}P]-3′-dNAD$^+$ as the substrate exclusively mono(ADP-ribosyl)ates the internal 22 kDa automodification domain of the enzyme. Panel A shows silver staining of intact PARP (lane 1) and PARP following partial proteolysis with either α-chymotrypsin (lane 2, closed arrows) or papain (lane 3, open arrows) as indicated under Experimental Procedures. Lane 4 of panel A shows the Coomassie Blue staining of PARP following sequential proteolytic degradation with α-chymotrypsin and papain. Panel B shows the autoradiograph of lanes 1−4 of panel A. The electrophoretic migration of the molecular mass markers is shown to the right of panel A. The relative molecular mass of the radiolabeled peptides of PARP following partial proteolysis is also shown to the left of panel B.

(Figures 1 and 2) results in the specific and time-dependent mono(ADP-ribosyl)ation of the enzyme. In fact, the enzyme becomes saturated with a maximum of 4 mol of 3′-dADP-ribose/mol of PARP (Figure 2B).

A major problem in studying the mechanism of PARP has been its ability to auto-poly(ADP-ribosyl)ate at multiple amino acid acceptor sites *(9, 10)*. The automodification of PARP results in auto-inactivation due to the electrostatic repulsion between the enzyme-bound polymers and DNA *(29, 30)*. Previous studies of the automodification reaction with high micromolar βNAD$^+$ concentrations have suggested that up to 15 *(9)* or 28 *(10)* polymers of ADP-ribose may be covalently bound to one molecule of PARP. However, the chain length (80 ADP-ribose units) and highly branched structure of the polymers synthesized *(9)* may have contributed to an overestimation of the total number of polymers bound per mole of enzyme. By contrast, our stoichiometric analysis of the mono(ADP-ribosyl)ation of PARP indicates that no more than four monomers of 3′-dADP-ribose are incorporated per mole of PARP. It should be noted, however, that we cannot distinguish between 4 mol of monomeric 3′-dADP-ribose/mol of PARP (scenario I) and 8 mol of initiated sites/PARP dimer (scenario II). The latter possibility may be particularly relevant if one subunit of dimeric PARP is the catalyst and the other subunit is the acceptor. This question remains unresolved.

Our experimental observation that increasing amounts of nicked dsDNA results in elevated levels of auto-mono(ADP-ribosyl)ation (Figure 3A) without any detectable ADP-ribose chain elongation (Figure 3B) is consistent with the hypothesis that the number of nicks or breaks on DNA not only controls ADP-ribose polymerization *(3)* but also determines the final number of ADP-ribose chains covalently attached to PARP. To our knowledge, this is the first time that it is demonstrated that nicked dsDNA stimulates the mono(ADP-ribosyl)-transferase activity associated with PARP. Of equal fundamental importance is our finding that the auto-mono(3′-dADP-ribosyl)ation catalyzed by PARP proceeded with second-order kinetics as a function of the enzyme (Figure 4A) in the absence of ADP-ribose chain elongation (Figure 4B). Therefore, our results are clearly consistent with the notion that the initiation reaction of poly(ADP-ribose) biosynthesis also involves two molecules of PARP and that this reaction is intermolecular in nature.

We have also conclusively determined that the four monomeric units of 3′-dADP-ribose covalently bound to PARP are directly linked to the internal 22 kDa automodification domain obtained following proteolytic treatment of mono(ADP-ribosyl)ated PARP with papain and α-chymotrypsin (Figure 5). While, the electrophoretic migration of mono(ADP-ribosyl)ated PARP in Figure 5A, lane 1, appears to trail to the origin, it should be pointed out that this polyacrylamide gel was stained with silver and radiolabeling of the enzyme was carried out in the presence of high molecular weight activated dsDNA *(3)*. Therefore, the stain smear observed in Figure 5A, lane 1, corresponds to silver-stained DNA. Indeed, no trailing is observed on the corresponding autoradiograph (Figure 5B, lane 1). A second point to analyze pertains to the small amount of radioactivity observed at the origin of the autoradiograph shown on Figure 5B, lane 4. While it might be suggested that this represents either oligo(ADP-ribosyl)ated PARP or radiolabeled protein that is resistant to proteolysis *(31)*, it should be pointed out that the data shown in Figures 1−4 are clearly consistent with the notion that the modified enzyme conjugates generated with 3′-dNAD$^+$ correspond to mono(ADP-ribosyl)ated PARP only. In addition, lanes 2 and 3 of the autoradiograph shown on Figure 5B illustrate that the proteolysis of mono-(ADP-ribosyl)ated PARP with either α-chymotrypsin (lane 2) or papain *(3)* is quantitative under the conditions used here. Finally, it should also be pointed out that the radiolabeled 66 kDa band observed on the autoradiograph of Figure 5B lane 4, is not visible on Figure 5A, lane 4, because

the total amount of this polypeptide is not sufficient for Coomassie Blue staining.

Also, the results described here with 3′-dNAD$^+$ as the enzyme automodification substrate show that at least 50% of the molecules of PARP become mono(3′-dADP-ribosyl)-ated. By comparison, Kameshita et al. *(27)*, who carried out the auto-poly(ADP-ribosyl)ation of PARP under suboptimal conditions to facilitate their proteolytic peptide mapping of PARP, observed that less than 10% of the PARP molecules were modified. In their experiments, they incubated pure enzyme with 2.4 μM NAD$^+$ at 0 °C for a few seconds to avoid the generation of PARP−(ADP-ribose)$_n$ conjugates that would stereochemically hinder the proteolytic activity of papain and/or α-chymotrypsin. Therefore, it is noteworthy to emphasize that despite the technical limitations at the time, their conclusions *(27)* agree very well with our results and we both identify the centrally located 22 kDa peptide domain as the main target for the ADP-ribose chain initiation reaction catalyzed by PARP. This conclusion is further supported by our previous findings that 3′-dADP-ribose-initiated chains are perfectly elongatable with a chase of high micromolar NAD$^+$ *(24)*. Further physicochemical and kinetic studies are underway in this laboratory to determine the chemical and regulatory mechanisms of poly(ADP-ribose) polymerase.

REFERENCES

1. Lautier, D., Lagueux, J., Thibodeau, J., Menard, L., and Poirier, G. G. (1993) *Mol. Cell. Biochem. 122*, 171−193.
2. deMurcia, G., and Menessier-deMurcia, J. (1994) *Trends Biochem. Sci. 19*, 172−176.
3. Benjamin, R. C., and Gill, D. M. (1980) *J. Biol. Chem. 255*, 10493−10501.
4. Gradwohl, G., Menessier-deMurcia, J., Molinete, M., Simonin, F., Koken, M., Hoeijmakers, J. H., and deMurcia, G. (1990) *Proc. Natl. Acad. Sci. U.S.A. 87*, 2990−2994.
5. Yoshihara, K., Hashida, T., Yoshihara, H. T., Tanaka, Y., and Oghushi (1977) *Biochem. Biophys. Res. Commun. 78*, 1281−1288.
6. Jump, D. B., and Smulson, M. (1980) *Biochemistry 19*, 1024−1030.
7. Adamietz, P., and Rudolph, A. (1984) *J. Biol. Chem. 259*, 6841−6846.
8. Adamietz, P. (1987) *Eur. J. Biochem. 169*, 365−372.
9. Kawaichi, M., Ueda, K., and Hayaishi, O. (1981) *J. Biol. Chem. 256*, 9483−9489.
10. Desmarais, Y., Menard, L., Lagueux, J., and Poirier, G. G. (1991*) Biochim. Biophys. Acta 1078*, 179−186.
11. Malanga, M., and Althaus, F. R. (1994) *J. Biol. Chem. 269*, 17691−17696.
12. Realini, C. A., and Althaus, F. R. (1992) *J. Biol. Chem. 267*, 18858−18865.
13. Menessier-deMurcia, J., Niedergang, C. P., Trucco, C., Ricoul, M., Dutrillaux, B., Oliver, J., Masson, M., Dierich, A., LeMeur, M., Walzinger, C., Chambon, P., and deMurcia, G. (1997) *Proc. Natl. Acad. Sci. U.S.A. 94*, 7303−7307.
14. LeCam, E., Fack, F., Menessier-deMurcia, J., Cognet, J. A. H., Barbin, A., Sarantoglou, V., Revet, B., Delain, E., and deMurcia, G. (1994) *J. Mol. Biol. 235*, 1062−1071.
15. Bauer, P. I., Buki, K. G., Hakam, A., and Kun, E. (1990) *Biochem. J. 270*, 17−26.
16. Mendoza-Alvarez, H., and Alvarez-Gonzalez, R. (1993) *J. Biol. Chem. 268*, 22575−22580.
17. Panzeter, P., and Althaus, F. R. (1994) *Biochemistry 33*, 9600−9605.
18. Alvarez-Gonzalez, R., and Mendoza-Alvarez, H. (1995) *Biochimie 77*, 403−407.
19. Zahradka, K., and Ebisuzaki, K. (1984) *Eur. J. Biochem. 142*, 503−509.
20. Alvarez-Gonzalez, R. (1988) *J. Chromatogr. 444*, 89−95.
21. Alvarez-Gonzalez, R., and Ringer, D. P. (1988) *FEBS Lett. 236*, 362−366, 1988.
22. Scovassi, A. I., Stefanini, M., and Bertazzoni, U. (1984) *J. Biol. Chem. 259*, 10973−10977.
23. Alvarez-Gonzalez, R. (1988) *J. Biol. Chem. 263*, 17690−17696.
24. Alvarez-Gonzalez, R., and Jacobson, M. K. (1987) *Biochemistry 26*, 3218−3224.
25. Nishikimi, M., Ogasawara, K., Kameshita, T., Taniguchi, T., and Shizuta, Y (1982) *J. Biol. Chem. 257*, 6102−605.
26. Kameshita, I., Matsuda, Z., Taniguchi, T., and Shizuta, Y. (1984) *J. Biol. Chem. 259*, 4770−4776.
27. Kameshita, I., Matsuda, M., Nishikimi, M., Ushiro, H., and Shizuta, Y. (1986) *J. Biol. Chem. 261*, 3863−3868.
28. Miwa, M., Saikawa, N., Yamaizumi, Z., Nishimura, S., and Sugimura, T. (1979) *Proc. Natl. Acad. Sci. U.S.A. 76*, 595−599.
29. Zahradka, P., and Ebisuzaki, K. (1982) *Eur. J. Biochem. 127*, 579−585.
30. Ferro, A., and Olivera, B. (1983) *J. Biol. Chem. 258*, 6000−6003.
31. Boulikas, T., and Poirier, G. G. (1992) *Biochem. Cell. Biol. 70*, 1258−1267.

BI982148P